frontiers | Frontiers in Earth Science

TYPE Original Research
PUBLISHED 08 September 2022
DOI 10.3389/feart.2022.981037

OPEN ACCESS

EDITED BY
Hu Li,
Southwest Petroleum University, China

REVIEWED BY
Hexin Huang,
Chang'an University, China
Pei Li,
SINOPEC Petroleum Exploration and Production Research Institute, China

*CORRESPONDENCE
Hui Xiao,
xiaohui@xsyu.edu.cn

†Present address:
Hui Xiao,
School of Earth Science and Engineering, Xi'an Shiyou University, Xi'an, China

SPECIALTY SECTION
This article was submitted to Structural Geology and Tectonics, a section of the journal Frontiers in Earth Science

RECEIVED 29 June 2022
ACCEPTED 12 August 2022
PUBLISHED 08 September 2022

CITATION
Xiao H, Xie N, Lu Y, Cheng T and Dang W (2022), Experimental investigation of pore structure and its influencing factors of marine-continental transitional shales in southern Yan'an area, ordos basin, China. *Front. Earth Sci.* 10:981037. doi: 10.3389/feart.2022.981037

Experimental investigation of pore structure and its influencing factors of marine-continental transitional shales in southern Yan'an area, ordos basin, China

Hui Xiao[1,2,3*†], Nan Xie[2,3], Yuanyuan Lu[4], Tianyue Cheng[2,3] and Wei Dang[2,3]

[1]The Key Laboratory of Unconventional Petroleum Geology, Oil & Gas Survey, China Geological Survey, Beijing, China, [2]School of Earth Sciences and Engineering, Xi'an Shiyou University, Xi'an, China, [3]Shaanxi Key Laboratory of Petroleum Accumulation Geology, Xi'an Shiyou University, Xi'an, China, [4]CNOOC Research Institute Ltd., Beijing, China

The intensive study of the pore structure and its controlling factors of shale reservoir has important guiding significance for further exploration and exploitation of shale gas. This work investigated the effects of organic and inorganic compositions on the development of pore structures of the Upper Permian Shanxi shale in the southern Yan'an area, Ordos Basin. Based on the results of high-pressure mercury intrusion, low-pressure N_2 and CO_2 adsorption and organic geochemical experiments, X-ray diffraction and scanning electron microscope observations, the mineral composition, pore structure and its influencing factors of the transitional shale were studied systematically. The results indicate that the total organic carbon (TOC) content of the shale is between 0.12% and 5.43%, with an average of 1.40%. The type of the organic matter (OM) belongs to Type III and has over maturity degree with an average R_o of 2.54%. An important character of this kind of shale is the large proportion of clay mineral content, which ranges from 40.70% to 87.00%, and with an average of 60.05%. Among them, illite and kaolinite are the main components, and they account for 36.6% and 36.7% of the total clay minerals respectively, followed by chlorite and illite/smectite (I/S) mixed layer. The quartz content is between 10.6% and 54.5%, with an average of 35.49%. OM (organic matter) pores are mostly circular bubble-shaped pores, and most of them are micropores, while inorganic pores are well developed and mainly contributed by clay mineral pores and have slit-type, plate-like and irregular polygon forms. Mesopores are the major contributor to pore volume (PV), while micropores contribute the least to PV. The contribution of micropores to the specific surface area (SSA) is greater than 61%, followed by mesopores. Macropores have almost no contribution to the development of SSA. OM pores are the main contributor to the total specific surface area of the shale, with an average contribution rate of 61.05%, but clay mineral pores contribute more to the total pore volumes. In addition, both the content of chlorite and illite/smectite (I/S) mixed layer is positively correlated with the volume ratio of mesopores. It was found that high TOC, I/S mixed layer and chlorite content are all favorable conditions for the target shale.

KEYWORDS
clay-rich shale, transitional shale, pore structure, controlling factors, ordos basin

Introduction

As the demand for fossil fuels increases, unconventional resources have attracted an increasing attention from many countries (Dang et al., 2022). In 2017, China's shale gas production reached $9\times10^{10}m^3$, occupying 6.09% of the whole country's natural gas production. The commercial exploitation of shale gas in the Fuling area, Sichuan Basin, has made great breakthroughs, and industrial gas flow has also been achieved in the Guizhou and Yunnan Provinces. In addition, shale gas exploration has been carried out in the Ordos Basin, Qaidam Basin and Songliao Basin in China (Chen et al., 2016; Dang et al., 2016; Sun et al., 2021).

At present, there are a lot of detailed research on the reservoir evaluation of marine and continental shales, however, there is a lack of systematic research in transitional shales. The transitional shales are widely distributed in different sedimentary strata in China (Jiang et al., 2015; Li et al., 2020a; Li et al., 2020b; Zhang et al., 2020). Compared with the marine strata, shale reservoirs in transitional shales are rich in clay minerals and usually have a high value for the maturity of organic matters (Jiang et al., 2015; Yang et al., 2016; Santosh and Feng., 2020; Zheng et al., 2020; Li et al., 2021a). Distributions of pore structure parameters, which are important of shale gas storage and flow, have been widely concerned and evaluated by many scholars. According to the International Union of Pure and Applied Chemistry Classification (IUPAC), shale pores are divided into micropores (<2 nm), mesopores (2–50 nm), and macropores (>50 nm) according to their pore size. Generally, micropores provide the main accumulation sites for adsorbed gas, while mesopores and macropores provide the main accumulation sites for free gas (Curtis et al., 2012; Sun et al., 2015; Zhao et al., 2020). Therefore, the quantitative characterization of pore structures of different sizes in shale gas is critical.

Organic matter and mineral components are the two main factors controlling the development of shale pore structures. Organic matter in shale controls the development of nanopores and is an important contributor to specific surface area and pore space, therefore, it is important for shale gas adsorption and storage (Loucks et al., 2009; Wang et al., 2020; Lan et al., 2021; Zhao et al., 2021). The mineral components of quartz, clay, and carbonate rocks are all related to the development of pores and fractures in shale. The feature of high clay mineral content cannot be ignored when studying the pore structures of the transitional shale (Dang et al., 2017; Guozhang Li et al., 2019; Ma et al., 2019; Yong Li et al., 2019; He et al., 2020).

As to the transitional shale reservoirs, many scholars have focused on the evaluation of reservoir properties, influencing factors of gas content and its accumulation conditions, and prediction of favorable areas (Dang et al., 2017; Xiong et al., 2017; Xi et al., 2018; Yin et al., 2018; Guozhang Li et al., 2019; Kun Yu et al., 2019; Ma et al., 2019; Qi et al., 2019; Yin and Gao 2019). However, the development characteristics of shale pore structures of transitional shale are still not clear.

This study takes the Upper Paleozoic Shanxi Formations in the Ordos Basin as an example and various testing methods have been used to quantify the shale pore structures. The main objectives are: 1) to understand the basic geochemistry, mineral composition characteristics, pore development types and pore distribution characteristics of the transitional shale in the study area; 2) to analyze the main controlling factors of the pore structures of the transitional shale.

Samples and methods

Preparation of clay-rich shale samples

The Ordos Basin is the second largest sedimentary basin in the central China. It is a typical craton basin where multiple prototype basins overlap. It includes six sub-level tectonic units (Figure 1A). Since the Late Paleozoic, the Ordos Basin has experienced many transgressions and tectonic changes affected by regional structure movement, basement faulting, and sea-level rising and falling. A thick marine-continental transitional stratum was deposited in the Carboniferous-Permian of the Upper Paleozoic. The shale gas-bearing strata from bottom to top are the Benxi Formation, the Taiyuan Formation and the Shanxi Formation, respectively (Figure 1B) (Yan et al., 2015). The sedimentary environments are dominated by marsh-lagoon facies and marine-continental transition delta facies. Sandstone, coal, and black shale are widely developed in the Shanxi Formation. The shale of the Shanxi Formation is dominated by clay minerals, with an average mass fraction of over 50% (Sun et al., 2017; Yin et al., 2019; Zhu et al., 2019).

The study area belongs to the southern of the Yishan Slope (Figure 1A). A total of 10 groups of core samples in the Shanxi Formation were collected from the Wells C88 and C89 for this study. The depth of the samples ranges from 2 271.5 to 2 437.4 m. Total organic carbon (TOC), vitrinite reflectance (R_o), full-rock and clay X-ray diffraction (XRD), field emission—scanning electron microscopy (FE-SEM), low-temperature CO_2 and N_2 adsorption and high-pressure mercury injection (MICP) experiments were used to analyze the pore structures of shale reservoirs in the study area. Organic petrography analysis including R_o and TOC test,

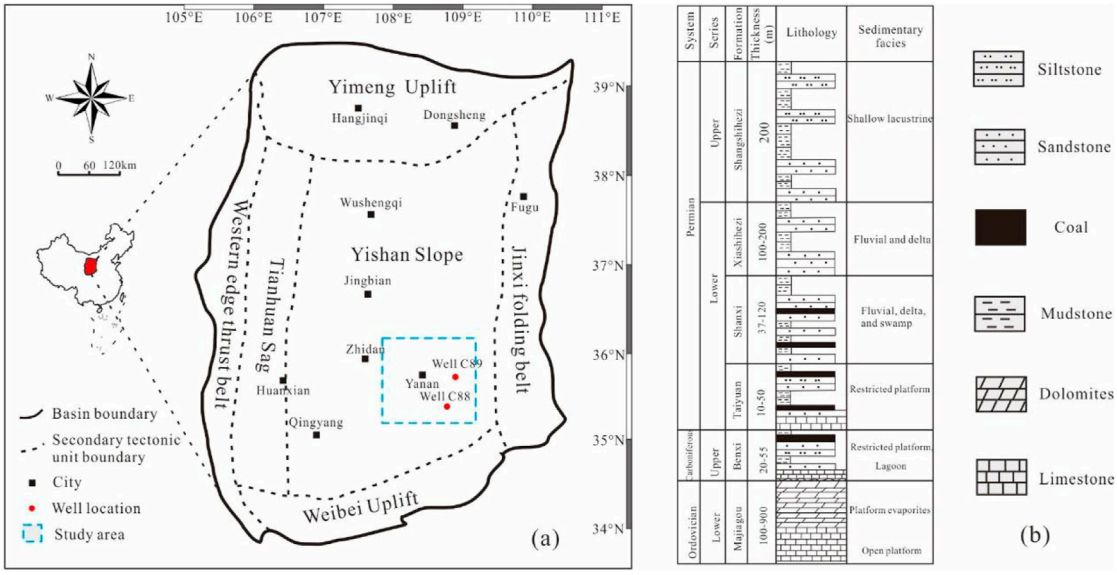

FIGURE 1
Location and well distribution of the study area **(A)** and generalized stratigraphic column of the Upper Paleozoic, Ordos Basin **(B)** (Modified after Yang et al., 2016).

and FE-SEM were all conducted at the Shaanxi Key Lab of Petroleum Accumulation Geology, Xi'an Shiyou University; the experiments of XRD, CO_2, and N_2 absorption analysis and MICP were performed by the Sichuan Province Key Laboratory of Shale Gas Evaluation and Exploration.

Experiment methods

The TOC content of the samples was determined using a carbon-sulfur analyzer (CS-230) from the American LECO Company based on the Chinese National Standards (GB/T19145-2003). Samples were milled and sieved to 100 mesh, and then 5 g powder sample were placed in HCl for 2 h to remove inorganic carbon and impurities and then washed with distilled water and dried. The R_o of the samples was examined using a Leitz MPV-SP photometer microscope according to the Chinses National standards (GB/T6948-1998). The test is performed at a temperature of 23°C ± 3°C, and the relative humidity is below 70%.

The whole rock and clay mineral compositions were analyzed by a D8 Discover X-ray diffractometer, following the Chinese Oil and Gas Industry Standards (SY/T 5163-2010). After crushing the sample particles to less than 200 mesh, 80 g sample were mixed with ethanol, ground into mortar, and placed on glass slides. The pretreated samples were scanned at rate of 4°/min, and the scanning range was 3–85°(2θ). The mineral content was semi-quantified using Jade ® software.

The FE-SEM of samples were determined using a TESCAN MALA3 LMH. Samples were observed under vacuum conditions with an acceleration voltage of 15 K_v and a resolution of 1 nm. In prior of SEM, the surfaces of the shale samples were etched *via* ion milling.

The low-temperature CO_2 adsorption and N_2 adsorption/desorption were performed on shale samples at 0°C and −195.8°C, respectively (2 g) using the Micromeritics ASAP 2460 specific surface analyzer. To characterize the overall size of the pores distributed in the shale samples, the SSA and PV distributions of micropores were obtained from the CO_2 adsorption data using the Density Function Theory (DFT) (Clarkson et al., 2013). The SSA distribution of mesopores and macropores were explained using the N_2 adsorption/desorption data by the Brunauer-Emmett-Teller (BET) model, and the PV distributions of pores ranging from 2–10 nm and 10–100 nm were obtained by the DFT and Barrett-Joyner-Halenda (BJH) models (Guozhang Li et al., 2019). In the past, the BJH, BET and DFT theory are the most used methods to extract the pore surface area and pore volume from the N_2 and CO_2 adsorption isotherms, and more importantly, these methods have been proved to be successful in characterizing the pore structures (Dang et al., 2020; Li et al., 2021b). MICP analysis were performed on the American Mike Auto Pore IV9520 type mercury pressure instrument. The maximum mercury inlet pressure is 227.4 MPa, the experimental interfacial tension σ is 480 dyn/cm, the wetting angle θ is 140°, and the mercury volume accuracy is 0.1 μl. The experiment is operated based on the Chinese Oil and Gas Industry Standards (SY/T 5346-2005).

TABLE 1 The mineral composition and geochemical parameters of transitional shale reservoirs in study area.

Samples	Depths (m)	TOC (%)	R_o (%)	Mineral composition (%)					
				Quartz	Clay	Illite	Kaolinite	I/S	Chlorite
A-1	2 271.45	1.56	2.43	29.4	69.2	23.46	20.01	16.56	8.97
A-2	2 284.62	0.82	2.23	24.8	76.3	27.36	30.40	6.84	11.40
A-3	2 293.00	1.24	2.46	36.1	59.1	18.29	31.27	4.72	4.72
A-4	2 301.77	0.62	2.39	39.3	58.8	22.04	23.78	4.06	8.12
A-5	2 304.31	0.72	2.72	31.2	69.2	24.84	28.98	4.83	10.35
A-6	2 306.69	0.80	2.53	21.2	79.5	21.33	41.87	8.69	7.11
A-7	2 431.09	0.11	—	10.6	87.0	36.54	18.27	13.05	19.14
A-8	2 433.52	5.42	2.44	27.4	58.9	20.30	19.72	4.64	13.34
A-9	2 435.84	1.23	—	24.7	68.4	29.24	21.08	4.08	13.60
A-10	2 437.41	0.86	—	28.4	67.1	29.48	15.41	16.75	5.36

Note: Clay content is absolute content.

Results

Mineral composition and organic geochemical characterization

The TOC content of the shale samples ranges from 0.11% to 5.42%, with an average of 1.34% (Table 1). Compared with previous research results, it is found that the organic matter content of the transitional shale varies greatly (Xiong et al., 2017; Xi et al., 2018; Gao, 2019; Guozhang Li et al., 2019; Ma et al., 2019). The range of R_o value ranges from 2.23% to 2.72%, with an average of 2.46% (Table 1), indicating that the shale samples in the study area are at over maturity stage, i.e., dry gas window (Nie et al., 2020). The shale in the study area and its vicinity mainly contains Type III kerogen and terrestrial microscopic components (vitrinite and inertinite) (Xi et al., 2017).

The XRD and clay analysis results show that the total clay content is distributed between 58.8% and 87.00%, with an average of 69.35%. Among clay minerals, illite and kaolinite have a relative high content, and their average value are 25.29% and 25.08% respectively. Followed by the chlorite and I/S contents, the average content are 10.21% and 8.42% respectively (Table 1). The quartz content ranges from 10.6% to 39.3%, with an average of 27.31%. It also contains a small amount of feldspar and pyrite. Compared with continental or marine shale, high clay mineral content has become another important feature of transitional shale (Xu et al., 2019a; Li et al., 2021a).

Studies on transitional shale found that clay minerals have a certain adsorption of organic matter. Organic matter can be attached to the surface of clay mineral particles, which is mainly manifested in a significant increase in the TOC content as the total clay mineral content in the shale increases (Dang et al., 2017; Hou et al., 2020). However, this study also found that with the increase of the TOC content, the clay mineral content decreases (Figure 2). After comparisons with previous studies of the transitional shale of the Shanxi Formation in the Ordos Basin and the marine shale of the Longmaxi Formation in Sichuan Basin, we found that the total clay minerals have a negative correlation with the TOC content (Xiong et al., 2017; Xu et al., 2019b; Xu and Gao., 2020). Further research is needed to confirm the correlation between the TOC and the total clay contents in different depositional environments.

Pore types

According to International Union of Pure and Applied Chemistry (IUPAC) classification, the N_2 adsorption curves of shale samples are mainly Type IV (Yong Li et al., 2019). When the relative pressure P/P_0 is in the range of 0.45–0.90, capillary condensation occurs in the curves and a hysteresis loop forms, indicating that there are many mesopores (2–50 nm) in the shale. When the relative pressure P/P_0 is small (<0.3), the adsorption curve changes gently with the increasing pressure. When P/P_0> 0.9, most samples show a steep upward trend with the increasing pressure.

The hysteresis loops in the N_2 adsorption curves are mainly H_3 and H_4 types, indicating that the pores in the shale are mostly slit-shaped and wedge-shaped pores. FE-SEM observations show that the shale pore types in the study area are mostly inorganic mineral pores such as clay mineral interlayer pores, intercrystalline pores, mineral intergranular pores, and intragranular dissolution pores (Figure 3). Figures 3A,B are pores related to clay minerals. This kind of pores are developed well and are mostly clay interlayer pores. The pore shape is mostly slit-shaped, the slit

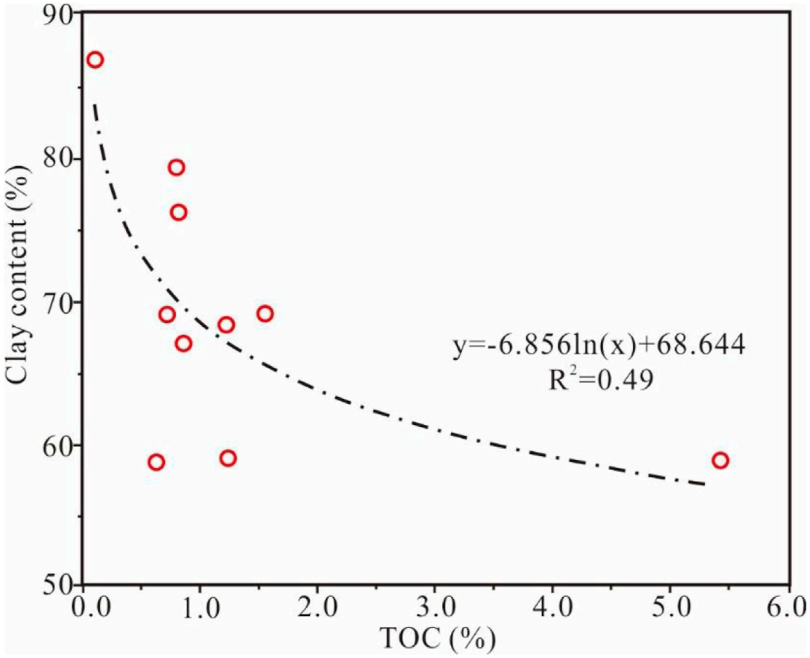

FIGURE 2
Relationship between shale TOC content and clay minerals.

width is mostly below 100 nm, and the slit length is mostly 2–3 μm. Figures 3C,D are pores related to brittle particles. This kind of pores are relatively less developed and are mainly intergranular and polygonal intergranular pores. The pore diameter of some intergranular pores reaches micron level, and a small number of particles develop intragranular dissolution pores. The contact slits between particles are mostly formed by the contact of brittle minerals and clay minerals, or by the density difference of different brittle minerals. From the FE-SEM observations, organic matter pores are less developed and are mostly shown as round bubbles. A few samples develop mesoporous organic pores, and the pore diameter can reach 10–20 nm (Figures 3E,F).

Pore structure characteristics

The distribution characteristics of the PV and the SSA of the 10 shale samples in the study area are listed in Table 2; Figure 4. The PV of micropores calculated by the DFT CO_2 and N_2 absorption data ranges from 0.000 63 cm^3/g to 0.007 13 cm^3/g, with an average of 0.002 47 cm^3/g and the SSA of micropores resulted from the BET CO_2 and N_2 absorption experiments varies between 2.054 m^2/g to 21.424 m^2/g, with an average of 7.564 m^2/g. The PV of mesopores calculated by the BJH N_2 absorption data is between 0.005 4 cm^3/g and 0.015 7 cm^3/g, with an average of 0.010 0 cm^3/g and the corresponding SSA is between 1.59 m^2/g and 5.88 m^2/g, with an average of 4.02 m^2/g. Macropores are characterized by the combination of N_2 adsorption and MICP data, while pores above 100 nm are based on MICP data (Yu et al., 2016). The PV of macropores range from 0.003 9 cm^3/g to 0.007 4 cm^3/g, with an average of 0.005 4 cm^3/g, and the corresponding SSA vary from 0.13 m^2/g to 0.28 m^2/g, with an average of 0.20 m^2/g. Combining with the pore characteristic distributions resulted from the CO_2, N_2 absorption, and MICP data, the average total PV is 0.017 cm^3/g, and the average total SSA is 11.79 m^2/g (Table. 2). The previous studies on the pore structures of transitional shale are consistent with the results of this paper (Cao et al., 2015; Wang et al., 2015).

Figure 4 shows that the total PV and SSA have no clear changing trend with the increase of TOC content. However, the PV and SSA proportion of micropores show a nonlinear increasing trend as the TOC content increases. The statistical results show that the main contributor of PV is mesopores, accounting for an average of 54.7% of the total PV, followed by the macropores, accounting for an average of 30.9% of the total PV. The micropores of PV, with an average of 14.4% of the total PV, takes the least proportion of PV, but SSA of the study shale is mainly dominated by the contribution of micropores, with an average 61.05% of the SSA. The SSA of the mesopores takes an average proportion of 36.9% of the total SSA.

According to statistics, the average volume of the mesopores accounts for 54.7% of the total pore volume, but the mesopore

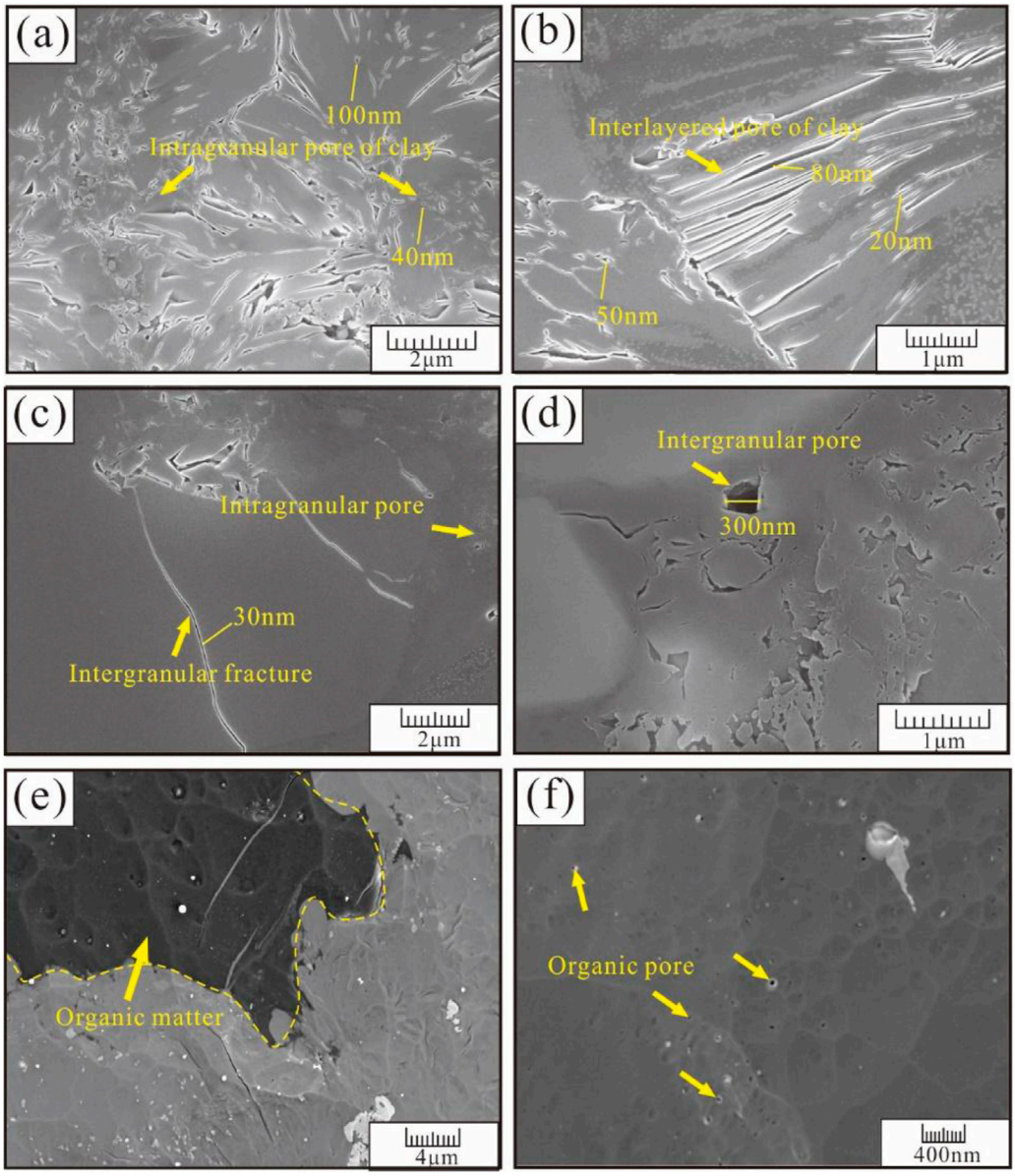

FIGURE 3
Development characteristics of different types of pores in shale reservoirs. **(A,B)** Clay mineral-related pores, the pores are relatively developed. Slit-shaped pores, strip-shaped interlayer pores, triangular and irregular polygonal intergranular pores and intragranular pores are developed; **(C,D)** Inorganic mineral-related pores. They are mainly composed of mineral intergranular pores and irregular residual intergranular pores, and there are a small number of intragranular dissolution pores with smaller pore size; **(E,F)** Organic matter-related pores (circled by yellow and white lines in the image). The pores are mostly round bubble pores. Organic matter pores are less developed and relatively small.

specific surface area only accounts for 36.97% of the total average surface area. The specific surface area is mainly dominated by the contribution of micropores, and the average specific surface area of micropores accounts for 61.05% of the total specific surface area. According to the average pore size calculation equation ($4V_p/A_s$) ×2 (V_p is the total pore volume and A_s is the total specific surface area) (Valenza et al., 2013), the average pore size of shale in the study area ranges from 5.73 to 18.89 nm. As the TOC content of the shale increases, the average pore size decreases rapidly and then becomes stable (Figure 5).

Pore-size distribution

It can be seen from Figure 6 that the interval of shale pore size distribution is wide. The micropores are mainly of the

TABLE 2 Pore structure parameters determined by CO_2, N_2 adsorption experiments and MICP experiments.

Sample	CO_2 and N_2 adsorption		MICP	CO_2 and N_2 adsorption		MICP	Total pore volume (cm^3 /g)	Total surface area (m^2 /g)	Average diameter (nm)
	DFT micropore volume (cm^3/g)	BJH mesopore volume (cm^3/g)	Macropore volume (cm^3/g)	BET micropore surface area (m^2/g)	BET mesopore surface area (m^2/g)	Macropore surface area (m^2/g)			
A-1	0.002 69	0.009 31	0.005 09	7.686	5.633	0.205	0.017 0	13.52	10.11
A-2	0.001 72	0.012 20	0.004 15	5.386	5.010	0.174	0.018 0	10.57	13.67
A-3	0.001 79	0.011 02	0.004 52	5.558	4.267	0.202	0.017 3	10.02	13.83
A-4	0.001 88	0.014 18	0.006 62	6.072	5.709	0.218	0.022 6	11.99	15.12
A-5	0.002 03	0.014 00	0.007 42	6.389	5.882	0.283	0.023 4	12.55	14.94
A-6	0.002 43	0.015 71	0.007 31	7.669	6.200	0.284	0.025 4	14.15	14.38
A-7	0.000 63	0.006 62	0.003 95	2.054	2.554	0.136	0.011 2	4.740	18.89
A-8	0.007 13	0.005 41	0.004 05	21.424	1.596	0.130	0.016 5	23.15	5.73
A-9	0.002 36	0.005 88	0.005 54	7.076	1.724	0.213	0.013 7	9.01	12.23
A-10	0.002 09	0.005 76	0.005 44	6.328	1.644	0.211	0.013 2	8.18	12.99

Note: Average diameter = (4 V_p/A_s) ×2 (V_p is total pore volume, A_s is total specific surface area).

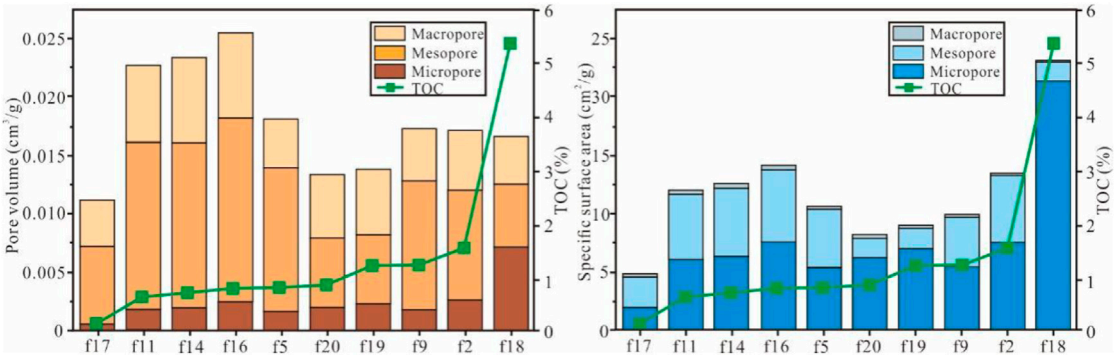

FIGURE 4
Distribution of pore volume and specific surface area of pores of different sizes in shale samples.

three-peak type, and the corresponding pore diameter ranges are 0.349 0 nm, 0.500 8 nm to 0.548 0 nm, and 0.785 5 nm to 0.859 4 nm. Because the lower limit of the CO_2 adsorption tests is 0.33 nm, then, during the pressure adsorption process, CO_2 will quickly occupy the pores, and will lead to the appearance of a peak of 0.33–0.4 nm (Kruk and Jaroniec 2001; Yuxi Yu et al., 2019), so the micropore distribution is mainly of a multi-modal type. The mesopores are of bimodal and unimodal types with peak pore sizes of 4 and 8 nm, respectively. The difference in pore size distribution of different samples indicates that the TOC content and mineral composition in shale are the main factors controlling the size and distribution of shale pores.

Discussions

Effect of organic matter content on pore structure

Organic matter not only affects the hydrocarbon generation potential in shale, but also generates many pores during the hydrocarbon generation process to provide storage space and migration channels for shale gas. Therefore, organic matter is one of the most important factors affecting the pore structures of shale reservoirs. Figure 7 shows the relationship between TOC and micropore pore volume. As the TOC content increases, the micropore volume increases, but it is negatively correlated with the

10.3389/feart.2022.981037

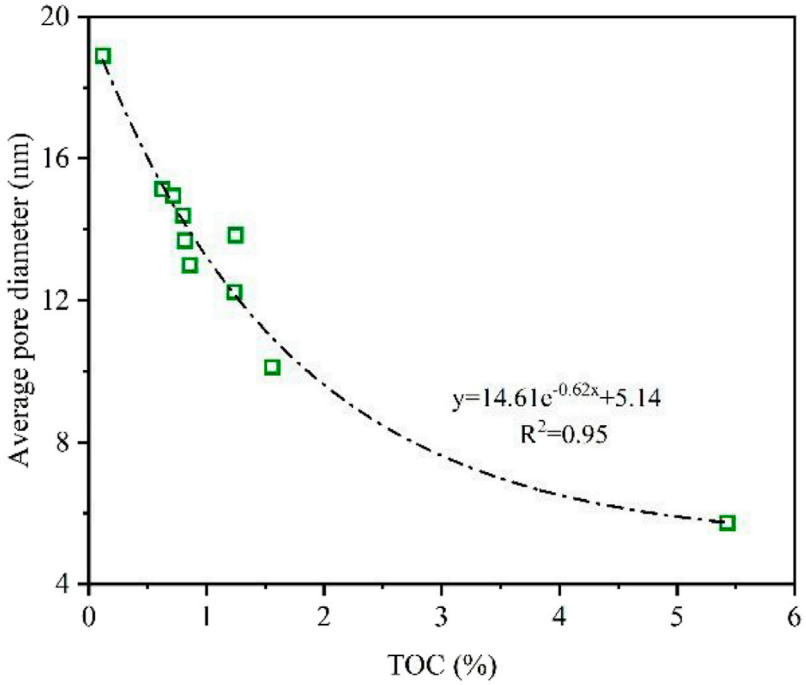

FIGURE 5
Relationship between TOC content and average pore diameter.

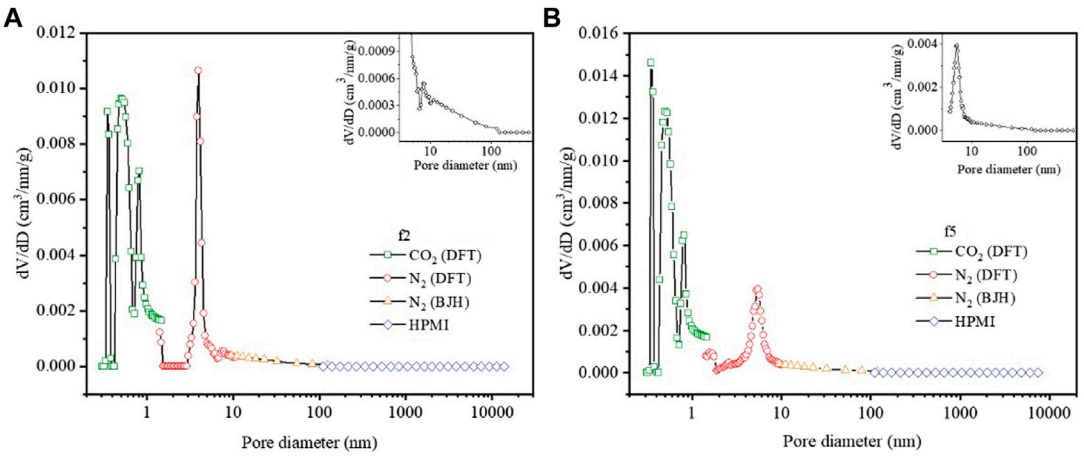

FIGURE 6
Shale pore size distribution combined with high pressure mercury intrusion, N_2 adsorption and CO_2 adsorption. Among them, the green dot pore size distribution curve is the interpretation results of CO_2 adsorption DFT model (<2 nm), the red dot pore size distribution curve is the interpretation results of N_2 adsorption DFT model (<10 nm), the yellow dot pore size distribution curve is the interpretation results of N_2 adsorption BJH model (<100 nm), and the blue point pore size distribution curve is the interpretation results of high pressure mercury intrusion Washburn equation (>100 nm). The inset in the upper right corner of the figure is an enlarged result of a curve with an aperture greater than 4 nm. **(A)** Sample f2; **(B)** Sample f5.

mesopores and macropores. In earlier studies conducted by Xiong et al. (2017) and Ma et al. (2019), they found that the TOC content in the marine-continental transitional shale mainly controls the development of mesopores, and the mesopore volume increases with the increasing TOC content. The rapid lithofacies changes, complex lithological combinations, and strong interlayer

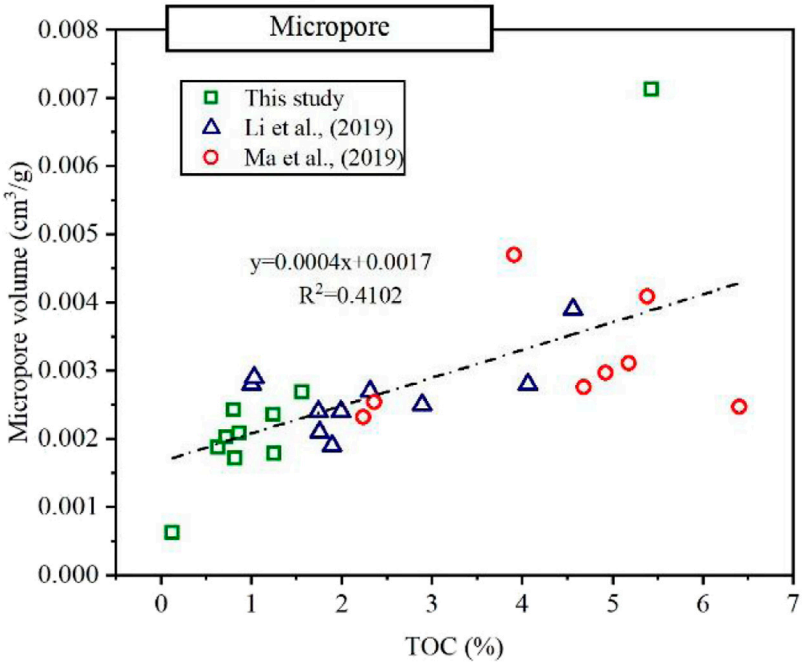

FIGURE 7
Relationship between TOC content and micropore pore volume in different marine-continental transitional shales. Notes: The blue dots are from the shale of the Shanxi Formation in the Linxing area of the Ordos Basin. Mature-high maturity shale. The clay minerals are mainly kaolinite (average 31%) (Yong Li et al., 2019). The red dots are from the Longtan Formation shale in Guizhou Province, which has a wide range of maturity (R_o is distributed between 0.86 and 2.04%). The clay minerals are mainly illite/smectite mixed layer (34% on average) (Ma et al., 2019).

heterogeneity of the marine-continental transitional shale can lead to inconsistent results. The analysis found that organic matter in the marine-continental transitional of different regions has a certain controlling effect on the degree of micropore development (Figure 7). According to Xi et al. (2018), maturity is the main factor controlling shale organic pore development, while the role of organic matter is relatively weak. The maturity controls the hydrocarbon generation potential of organic matter. When the organic matter enters the main hydrocarbon generation stage (the coal-bearing stratum Ro ranges from 0.75 to 0.9), the shale hydrocarbon generation potential is great, and the organic matter can generate a lot of pores. With the increase of TOC content, the decrease in total porosity is mainly due to two reasons. On the one hand, with the increase of organic matter, the compressibility of shale increases, and the filling of organic matter with pores leads to a decrease in pore volume (Xiong et al., 2017). On the other hand, the marine-continental transitional shale is mainly Type III kerogen. Compared with Types I and II, its macromolecular structures and chemical properties are relatively stable, which makes it difficult to change the structures of organic matter during pyrolysis and it is impossible to generate pores. Moreover, this type of kerogen is mainly gas-producing and has low hydrocarbon generation potential, which limits the development of organic matter pores. Organic matter pores are less developed and are mostly micropores. Mesopores and macropores are relatively undeveloped (Yang et al., 2016). FE-SEM observations showed that a small amount of mesoporous organic pores are developed in the shale in the study area (Figure 3F). The macropores are negatively correlated with the organic matter content or the correlation is not obvious, indicating that the marine-continental transitional shale is different from the marine shale. Organic matter in transitional shale is not related to the degree of macropore development. Previous studies have also shown that the macropores of the marine-continental transitional shales are mainly related to clay and brittle minerals (Ma et al., 2019).

The total specific surface area in the shale has a significant positive correlation with the TOC content, with R^2 of 0.64 (Figure 8A). It shows that with the increase of the TOC content, the specific surface area in shale increases. This is mainly because, compared with other pores, organic matter pores are mostly porous media with a large specific surface area during the generation and discharge of hydrocarbons (Dang et al., 2017). The TOC content has a significant positive correlation with the volume and specific surface area of the micropores, indicating that organic pores are mostly micropores (Figure 7 and Figure 8B), and the micropores have a larger specific surface area than the mesopores and macropores. Therefore, as the TOC content increases, the total pore specific surface area also tends to increase. However, the

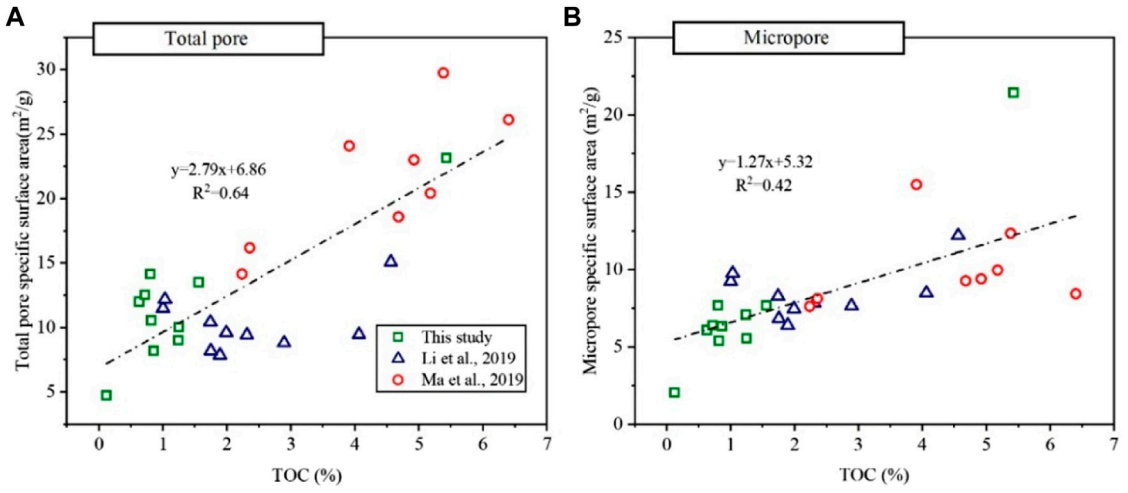

FIGURE 8
Relationship between TOC and pore specific surface area of marine-continental transitional shales in different regions. **(A)** Total pore; **(B)** Micropore.

relationship between the specific surface area of mesopores and macropores and the content of TOC is not obvious. The thermal evolution stage of organic matter has certain influence on the development of organic pores in transitional shale. Mature to highly mature samples have a higher degree of pore development (Guozhang Li et al., 2019). However, the Shanxi Formation shale in the Qinshui Basin has reached the over-mature stage. At this time, on the one hand, the organic hydrocarbon generation capacity is weak and there are no large pores, and some pores are destroyed due to reduced pore pressure (Zhang et al., 2019); on the other hand, over-mature shale leads to light hydrocarbon generation, organic carbonization and porosity reduction (Zhao et al., 2016).

Effect of minerals on pore structure

Due to the special structures and physical-chemical properties of clay minerals, pores of different shapes and sizes will be formed, and some cracks will develop. Diagenesis and sedimentary environment are two important factors controlling the type and combination of clay minerals. Different types of clay mineral crystals have different pore structures (Chalmers and Bustin, 2007; Chen et al., 2016). With the increase of the clay mineral content in the shale reservoir, the total PV shows an increasing trend (Figure 9), the mesopore and macropore volume also shows an increasing trend, while the micropores shows the opposite changing trend. This indicates that the clay minerals in the transitional shales affect the development of the total PV but have less influence on the development of micropores. According to Guozhang Li et al. (2019), the total clay content shows positive correlation with the PV of mesopores. Analyzed the characteristics of pure clay minerals and concluded that interlayer and intercrystalline pores were developed in the I/S mixed layers. These two types of pores are mainly medium to large pores with pore diameters of 1–6 nm and 20–100 nm, respectively, and the average pore diameters are 3.5 and 55 nm. Intercrystalline pores are mainly deceloped in chlorite. These pores are mesopores and macropores with a pore size distribution of 20–100 nm. The above analysis shows that different types of clay minerals develop pores of different sizes, and they are mostly mesopores and macropores. Therefore, clay content has a positive correlation with the PV except micropores.

With the increase of chlorite and I/S content in the shale reservoir, the mesopore volume increases significantly (Figure 10), but the content of kaolinite has a negative correlation with the mesopore volume. There was no significant correlation between the illite content and the mesopore pore volume. This indicates that chlorite and I/S contents are the main contributors to the mesopores. Research by Yang et al. (2016) suggested that I/S and illite in the transitional shale mainly affect the pore structures of the reservoir, while kaolinite and chlorite have a negative correlation with PV. Yong Li et al. (2019) believed that chlorite in clay minerals is the main factor affecting the pore structures of the transitional shales. It is obvious that different scholars have obtained inconsistent results when studying the effect of clay minerals on pore structures in transitional shales. Generally, compaction and different diagenetic evolution are the main factors that cause differences in shale clay mineral types and contents (Fu et al., 2015). Clay minerals are gradually transformed into relatively stable types, which changes the

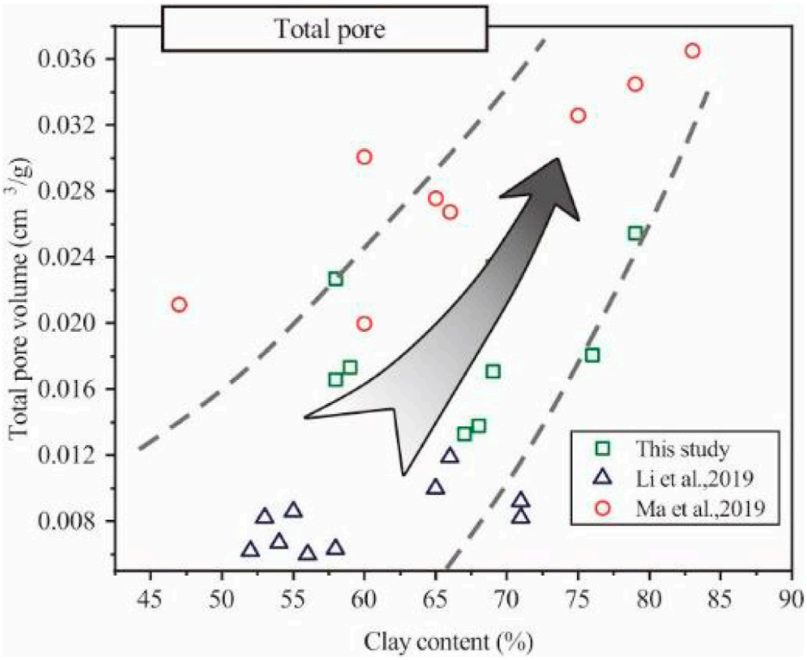

FIGURE 9
Correlation between total clay mineral content and pore volume in the marine-continental transitional shale in different regions.

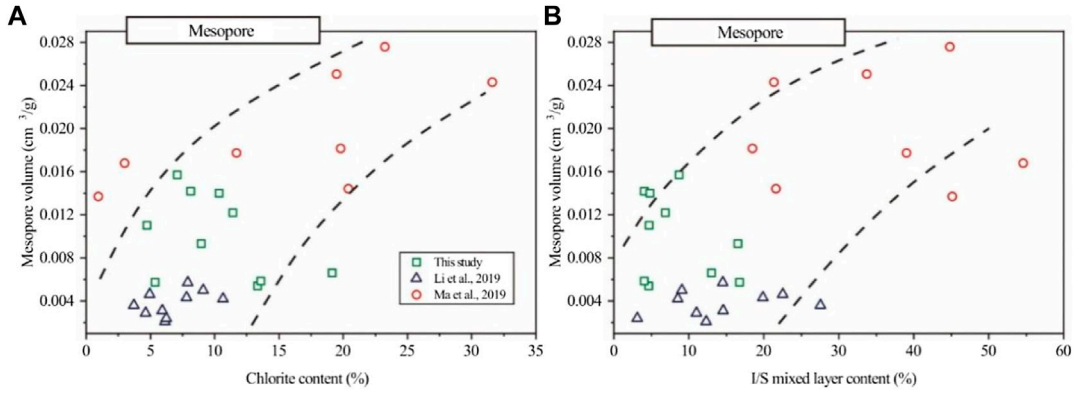

FIGURE 10
Correlation between clay minerals and mesopore volume in different marine-continental transitional shales. **(A)** Relationship between chlorite content and mesopore volume; **(B)** Relationship between I/S mixed layer content and mesopore volume.

molecular structures between layers, and the clay pores will change accordingly affected by the diagenetic evolutions. However, the research of different scholars does not deny the contribution of intercrystalline pores to the shale reservoir pores during different diagenetic stages (Chen et al., 2016). These studies suggested that the negative correlation between clay mineral types and PV was caused by the negative correlation between different clay minerals.

Brittle minerals in inorganic minerals such as quartz, feldspar, pyrite, and carbonate rocks are other factors that affect pore development in shale. The brittle mineral pores are greatly affected by the diagenesis during the sedimentation and burial. For example, compaction, pressure dissolution, cementation, and dissolution, all can cause the change of the development of theses pores. Figure 11 shows a weakly negative correlation between brittle minerals and the total pore volume. With the increase of brittle

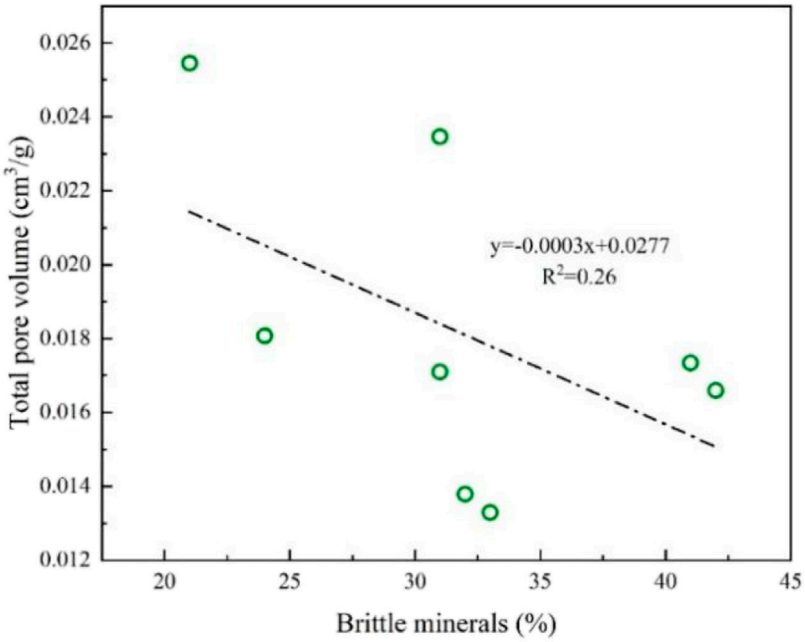

FIGURE 11
Correlation between brittle minerals and total pore volume in shale. Notes: Brittle minerals include quartz, feldspar, calcite, pyrite, and siderite.

mineral content, the total pore volume in the shale decreased slightly. This is mainly because the shale is very dense, and the acidic or alkaline fluids in the shale cannot dissolve quartz, feldspar and carbonate minerals, thus the dissolution pores are not developed. At the same time, secondary enlargement of quartz will also occupy pore spaces, thus leading to a decrease in the number of pores in shale (Kong et al., 2016).

Implications for favorable area prediction of transitional shale gas

Organic matter characteristics and mineral composition are two important parameters in the exploration and evaluation of shale gas reservoir sweet spots. The content of TOC in shale controls the degree of micropore development. Moreover, due to the hydrophilic nature of organic matter and strong intermolecular forces in micropores (Liang et al., 2016), TOC is also an important factor influencing methane adsorption capacity of shale reservoirs. The micropores contribute more to the specific surface area of shale. High TOC content increases the proportion of micropores and specific surface area in shale and can lead to the increase of the amount of shale gas adsorption. At the same time, TOC also provides a favorable location for shale gas storage. The composition of clay minerals is also an important factor that cannot be ignored. Different clay mineral contents and types have a greater impact on the pore structures of shale reservoir. High clay mineral contents provide more mesopores and macropores, and the total pore volume increases as well. When the organic matter content is low, mesopores in shales with high I/S and chlorite contents in clay minerals develop, which provides a favorable location for shale gas migration and accumulation. Therefore, the TOC content and the type and content of clay minerals are two important factors in the prediction and evaluation of sweet spots in the Upper Paleozoic clay-rich marine-continental transitional shale of the Ordos Basin.

Conclusion

- The pores in the marine-continental transitional shale in the Shanxi Formation, Ordos Basin are mostly slit-type and plate-type inorganic pores. Affected by the type of organic matter, organic matter has fewer pores and is mainly microporous, followed by a small number of mesopores. These pores are mostly bubble-like pores. Organic matter pores are the main contributors to specific surface area, with an average of 61.05%. With the increase of TOC content, the micropore volume and specific surface ratio in the reservoir increased significantly.
- For the marine-continental transitional clay-rich shale, clay mineral pores are the main pore types in inorganic pores, including clay interlayer pores, clay mineral intergranular pores, and inter-crystalline pores. With the increase of total clay content, the volume of total pores, mesopores and macropores in shale increased significantly. Chlorite and

I/S content have a greater impact on the pore development of clay minerals, followed by kaolinite and illite. Due to the special characteristics of shale and complex compaction and cementation, brittle mineral pores do not develop.

- Both TOC and clay minerals significantly affect the pore structure and methane adsorption capacity of marine-continental transitional clay-rich shale. Under the conditions of high TOC content, high I/S and chlorite content, micropores and mesopores in shale are relatively developed, and the reservoir pore space and adsorption capacity are large, which provide favorable conditions for shale gas accumulation (Li, 2021; Li, 2022).

Data availability statement

The original contributions presented in the study are included in the article/supplementary material, further inquiries can be directed to the corresponding author.

Author contributions

HX is responsible for the idea and writing of this paper, and TC and HW are responsible for the data interpretation.

Funding

This study was supported by Research on Clastic Sedimentology and Reservoir Evaluation (2019QNKYCXTD05).

Conflict of interest

YL is employed by the CNOOC Research Institute Ltd.

The remaining authors declare that the research was conducted in the absence of any commercial or financial relationships that could be construed as a potential conflict of interest.

Publisher's note

References

Cao, T., Song, Z., Wang, S., and Xia, J. (2015). A comparative study of the specific surface area and pore structure of different shales and their kerogens. *Sci. China Earth Sci.* 58, 510–522. doi:10.1007/s11430-014-5021-2

Chalmers, G. R. L., and Bustin, R. M. (2007). The organic matter distribution and methane capacity of the Lower Cretaceous strata of Northeastern British Columbia, Canada. *Int. J. Coal Geol.* 70 (1), 223–239. doi:10.1016/j.coal.2006.05.001

Chen, Q., Zhang, J., Tang, X., Dang, W., Li, Z., Liu, C., et al. (2016). Pore structure characterization of the lower permian marine-continental transitional black shale in the southern north China basin, Central China. *Energy fuels.* 30 (12), 10092–10105. doi:10.1021/acs.energyfuels.6b01475

Clarkson, C., Solano, N., Bustin, R., Bustin, A. M. M., Chalmers, G., He, L., et al. (2013). Pore structure characterization of North American shale gas reservoirs using USANS/SANS, gas adsorption, and mercury intrusion. *Fuel* 103, 606–616. doi:10.1016/j.fuel.2012.06.119

Curtis, M., Cardott, B., Sondergeld, C., and Rai, C. (2012). Development of organic porosity in the Woodford Shale with increasing thermal maturity. *Int. J. Coal Geol.* 103, 26–31. doi:10.1016/j.coal.2012.08.004

Dang, W., Zhang, J., Tang, X., Chen, Q., Han, S., Li, Z., et al. (2016). Shale gas potential of lower Permian marine–continental transitional black shales in the Southern North China Basin, central China: Characterization of organic geochemistry. *J. Nat. Gas Sci. Eng.* 28, 639–650. doi:10.1016/j.jngse.2015.12.035

Dang, W., Zhang, J., Wei, X., Tang, X., Chen, Q., Li, Z., et al. (2017). Geological controls on methane adsorption capacity of Lower Permian transitional black shales in the Southern North China Basin, Central China: Experimental results and geological implications. *J. Petroleum Sci. Eng.* 152, 456–470. doi:10.1016/j.petrol.2017.03.017

Dang, W., Zhang, J., Nie, H., Wang, F., Tang, X., Wu, N., et al. (2020). Isotherms, thermodynamics and kinetics of methane-shale adsorption pair under supercritical condition: Implications for understanding the nature of shale gas adsorption process. *Chem. Eng. J.* 383, 123191. doi:10.1016/j.cej.2019.123191

Dang, W., Nie, H., Zhang, J., Tang, X., Jiang, S., Wei, X., et al. (2022). Pore-scale mechanisms and characterization of light oil storage in shale nanopores: New method and insights. *Geosci. Front.* 13 (5), 101424. doi:10.1016/j.gsf.2022.101424

Fu, C. Q., Zhu, Y. M., and Chen, S. (2015). Diagenesis controlling mechanism of pore characteristics in the Qiongzhusi Formation Shale. *J. China Coal Geol.* 40, 439–448. doi:10.13225/j.cnki.jccs.2014.1588

Gao, F. (2019). Use of numerical modeling for analyzing rock mechanic problems in underground coal mine practices. *J. Min. Strata Control Eng.* 1 (1), 013004. doi:10.13532/j.jmsce.cn10-1638/td.2019.02.009

Guozhang Li, G., Qin, Y., Wu, M., Zhang, B., Wu, X., Tong, G., et al. (2019). The pore structure of the transitional shale in the Taiyuan formation, Linxing area, Ordos Basin. *J. Petroleum Sci. Eng.* 181, 106183–106186. doi:10.1016/j.petrol.2019.106183

He, X., Zhang, P., He, G., Gao, Y., Liu, M., Zhang, Y., et al. (2020). Evaluation of sweet spots and horizontal-well-design technology for shale gas in the basin-margin transition zone of southeastern Chongqing, SW China. *Energy Geosci.* 1 (3–4), 134–146. doi:10.1016/j.engeos.2020.06.004

Hou, E., Cong, T., and Xie, X. (2020). Ground surface fracture development characteristics of shallow double coal seam staggered mining based on particle flow. *J. Min. Strata Control Eng.* 2 (1), 013521. doi:10.13532/j.jmsce.cn10-1638/td.2020.01.002

Jiang, S., Xu, Z., Feng, Y., Zhang, J., Cai, D., Chen, L., et al. (2015). Geologic characteristics of hydrocarbon-bearing marine, transitional and lacustrine shales in China. *J. Asian Earth Sci.* 115, 404–418. doi:10.1016/j.jseaes.2015.10.016

Kong, L., Wan, M., Yan, Y., Zou, C., Liu, W., Tian, C., et al. (2016). Reservoir diagenesis research of silurian Longmaxi Formation in Sichuan Basin, China. *J. Nat. Gas Geoscience* 23, 203–211. doi:10.1016/j.jnggs.2016.08.001

Kruk, M., and Jaroniec, M. (2001). Gas adsorption characterization of ordered Organic–Inorganic nanocomposite materials. *Chem. Mat.* 13, 3169–3183. doi:10.1021/cm0101069

Kun Yu, K., Shao, C., Ju, Y., and Qu, Z. (2019). The genesis and controlling factors of micropore volume in transitional coal-bearing shale reservoirs under different sedimentary environments. *Mar. Petroleum Geol.* 102, 426–438. doi:10.1016/j.marpetgeo.2019.01.003

Lan, S. R., Song, D. Z., Li, Z. L., and Liu, Y. (2021). Experimental study on acoustic emission characteristics of fault slip process based on damage factor. *J. Min. Strata Control Eng.* 3 (3), 033024. doi:10.13532/j.jmsce.cn10-1638/td.20210510.002

Li, Y. (2021). Mechanics and fracturing techniques of deep shale from the Sichuan Basin, SW China. *Energy Geosci.* 2 (1), 1–9. doi:10.1016/j.engeos.2020.06.002

Li, H. (2022). Research progress on evaluation methods and factors influencing shale brittleness: A review. *Energy Rep.* 8, 4344–4358. doi:10.1016/j.egyr.2022.03.120

Li, Y., Zhou, D. H., Wang, W. H., Jiang, T. X., and Xue, Z. J. (2020a). Development of unconventional gas and technologies adopted in China. *Energy Geosci.* 1 (1–2), 55–68. doi:10.1016/j.engeos.2020.04.004

Li, L., Zhang, X., and Deng, H. (2020b). Mechanical properties and energy evolution of sandstone subjected to uniaxial compression with different loading rates. *J. Min. Strata Control Eng.* 2 (4), 043037. doi:10.13532/j.jmsce.cn10-1638/td.20200407.001

Li, P., Zhang, J., Rezaee, R., Dang, W., Tang, X., Nie, H., et al. (2021a). Effect of adsorbed moisture on the pore size distribution of transitional shales: Insights from clay swelling and lithofacies difference. *Appl. Clay Sci.* 34, 1–10. doi:10.1016/j.clay.2020.105926

Li, P., Zhang, J., Rezaee, R., Dang, W., Li, X., Fauziah, C., et al. (2021b). Effects of swelling-clay and surface roughness on the wettability of transitional shale. *J. Petroleum Sci. Eng.* 196, 108007. doi:10.1016/j.petrol.2020.108007

Liang, L., Xiong, J., Liu, X., and Luo, D. (2016). An investigation into the thermodynamic characteristics of methane adsorption on different clay minerals. *J. Nat. Gas Sci. Eng.* 33, 1046–1055. doi:10.1016/j.jngse.2016.06.024

Loucks, R., Reed, R., Ruppel, S., and Jarvie, D. (2009). Morphology, genesis, and distribution of nanometer-scale pores in siliceous mudstones of the mississippian barnett shale. *J. Sediment. Res.* 79, 848–861. doi:10.2110/jsr.2009.092

Ma, X., Guo, S., Shi, D., Zhou, Z., and Liu, G. (2019). Investigation of pore structure and fractal characteristics of marine-continental transitional shales from Longtan Formation using MICP, gas adsorption, and NMR (Guizhou, China). *Mar. Petroleum Geol.* 107, 555–571. doi:10.1016/j.marpetgeo.2019.05.018

Nie, H., Li, D., Liu, G., Lu, Z., Hu, W., Wang, R., et al. (2020). An overview of the geology and production of the Fuling shale gas field, Sichuan Basin, China. *Energy Geosci.* 1 (3–4), 147–164. doi:10.1016/j.engeos.2020.06.005

Qi, Y., Ju, Y., Huang, C., Zhu, H., Bao, Y., Wu, J., et al. (2019). Influences of organic matter and kaolinite on pore structures of transitional organic-rich mudstone with an emphasis on S2 controlling specific surface area. *Fuel* 237, 860–873. doi:10.1016/j.fuel.2018.10.048

Santosh, M., and Feng, Z. Q. (2020). New horizons in energy geoscience. *Energy Geosci.* 1 (1–2), 1. doi:10.1016/j.engeos.2020.05.005

Sun, M., Yu, B., Hu, Q.-H., Chen, S., Xia, W., and Ye, R. (2015). Nanoscale pore characteristics of the lower cambrian niutitang Formation shale: A case study from well yuke #1 in the southeast of chongqing, China. *Int. J. Coal Geol.* 154, 16–29. doi:10.1016/j.coal.2015.11.015

Sun, Z., Wang, Y., Wei, Z., Zhang, M., Wang, D., Wang, Z., et al. (2017). Shale gas content and geochemical characteristics of marine-continental transitional shale: A case from the Shanxi Formation of Ordos Basin. *J. China Univ. Min. Technol.* 46 (4), 859–868. doi:10.13247/j.cnki.jcumt.000663

Sun, C., Nie, H., Dang, W., Chen, Q., Zhang, G., Li, W., et al. (2021). Shale gas exploration and development in China: Current status, geological challenges, and future directions. *Energy fuels.* 35 (8), 6359–6379. doi:10.1021/acs.energyfuels.0c04131

Valenza, J. J., Drenzek, N., Marques, F., Pagels, M., and Mastalerz, M. (2013). Geochemical controls on shale microstructure. *Geology* 41 (5), 611–614. doi:10.1130/g33639.1

Wang, G., Ju, Y., Yan, Z., and Li, Q. (2015). Pore structure characteristics of coal–bearing shale using fluid invasion methods: A case study in the huainan–huaibei coalfield in China. *Mar. Petroleum Geol.* 62, 1–13. doi:10.1016/j.marpetgeo.2015.01.001

Wang, H., Shi, Z., Zhao, Q., Liu, D., Sun, S., Guo, W., et al. (2020). Stratigraphic framework of the Wufeng-Longmaxi shale in and around the Sichuan Basin, China: Implications for targeting shale gas. *Energy Geosci.* 1 (3–4), 124–133. doi:10.1016/j.engeos.2020.05.006

Xi, Z., Tang, S., Zhang, S., and Li, J. (2017). Nano-Scale pore structure of marine-continental transitional shale from liulin area, the eastern margin of Ordos Basin, China. *J. Nanosci. Nanotechnol.* 17, 6109–6123. doi:10.1166/jnn.2017.14501

Xi, Z., Tang, S., Wang, J., Yang, G., and Li, L. (2018). Formation and development of pore structure in marine-continental transitional shale from northern China across a maturation gradient: Insights from gas adsorption and mercury intrusion. *Int. J. Coal Geol.* 200, 87–102. doi:10.1016/j.coal.2018.10.005

Xiong, F., Jiang, Z., Li, P., Wang, X., Bi, H., Li, Y., et al. (2017). Pore structure of transitional shales in the Ordos Basin, NW China: Effects of composition on gas storage capacity. *Fuel* 206, 504–515. doi:10.1016/j.fuel.2017.05.083

Xu, H., Zhou, W., Hu, Q., Xia, X., Zhang, C., and Zhang, H. (2019a). Fluid distribution and gas adsorption behaviors in over-mature shales in southern China. *Mar. Petroleum Geol.* 109, 223–232. doi:10.1016/j.marpetgeo.2019.05.038

Xu, H., Zhou, W., Zhang, R., Liu, S., and Zhou, Q. (2019b). Characterizations of pore, mineral and petrographic properties of marine shale using multiple techniques and their implications on gas storage capability for Sichuan Longmaxi gas shale field in China. *Fuel* 241, 360–371. doi:10.1016/j.fuel.2018.12.035

Xu, N., and Gao, C. (2020). Study on the special rules of surface subsidence affected by normal faults. *J. Min. Strata Control Eng.* 2 (1), 011007. doi:10.13532/j.jmsce.cn10-1638/td.2020.01.011

Yan, D., Huang, W., and Zhang, J. (2015). Characteristics of marine continental transitional organic rich shale in the Ordos Basin and its shale gas significance. *Earth Sci. Froniters* 22 (6), 197–206. doi:10.13745/j.esf.2015.06.015

Yang, C., Zhang, J., Tang, X., Ding, J., Zhao, Q., Dang, W., et al. (2016). Comparative study on micro-pore structure of marine, terrestrial, and transitional shales in key areas, China. *Int. J. Coal Geol.* 171, 76–92. doi:10.1016/j.coal.2016.12.001

Yin, S., and Gao, Z. (2019). Numerical study on the prediction of "sweet spots" in a low efficiency-tight gas sandstone reservoir based on a 3D strain energy model. *IEEE Access* 7, 117391–117402. doi:10.1109/access.2019.2933450

Yin, S., Lv, D., and Ding, W. (2018). New method for assessing microfracture stress sensitivity in tight sandstone reservoirs based on acoustic experiments. *Int. J. Geomech.* 18 (4), 1–16. doi:10.1061/(asce)gm.1943-5622.0001100

Yin, S., Tian, T., and Wu, Z. (2019). Developmental characteristics and distribution law of fractures in a tight sandstone reservoir in a low-amplitude tectonic zone, eastern Ordos Basin, China. *Geol. J.* 54 (6), 1546–1562. doi:10.1002/gj.3521

Yong Li, Y., Wang, Z., Pan, Z., Niu, X., Yu, Y., and Meng, S. (2019). Pore structure and its fractal dimensions of transitional shale: A cross-section from east margin of the Ordos Basin, China. *Fuel* 241, 417–431. doi:10.1016/j.fuel.2018.12.066

Yu, Y., Luo, X., Lei, Y., Chen, M., Wang, X., and Zhang, L. (2016). Characterization of lacustrine shale pore structure: An example from the upper-triassic yanchang formation, Ordos Basin. *Nat. Gas. Geosci.* 27 (4), 716–726. doi:10.11764/j.issn.1672-1926.2016.04.0716

Yuxi Yu, Y., Luo, X., Wang, Z., Cheng, M., Lei, Y., Zhang, L., et al. (2019). A new correction method for mercury injection capillary pressure (MICP) to characterize the pore structure of shale. *J. Nat. Gas Sci. Eng.* 68, 102896–102896. doi:10.1016/j.jngse.2019.05.009

Zhang, M., Fu, X., Zhang, Q., and Cheng, W. (2019). Research on the organic geochemical and mineral composition properties and its influence on pore structure of coal-measure shales in Yushe-Wuxiang Block, South Central Qinshui Basin, China. *J. Petroleum Sci. Eng.* 34, 1–7. doi:10.1016/j.petrol.2018.10.079

Zhang, J., Tang, X., Huo, Z., Li, Z., Lee, E., Luo, K. Y., et al. (2020). Assessment of shale gas potential of the lower Permian transitional Shanxi-Taiyuan shales in the southern North China Basin. *Aust. J. Earth Sci.* 68, 262–284. doi:10.1080/08120099.2020.1762737

Zhao, W., Li, J., Yang, T., Wang, S., and Huang, J. (2016). Geological difference and its significance of marine shale gases in South China. *Petroleum Explor. Dev.* 43, 547–559. doi:10.1016/s1876-3804(16)30065-9

Zhao, Z., Wu, K., Fan, Y., Guo, J., Zeng, B., and Yue, W. (2020). An optimization model for conductivity of hydraulic fracture networks in the Longmaxi shale, Sichuan basin, Southwest China. *Energy Geosci.* 1 (1–2), 47–54. doi:10.1016/j.engeos.2020.05.001

Zhao, K. K., Jiang, P. F., Feng, Y. J., Sun, X. D., Cheng, L. X., and Zheng, J. W. (2021). Investigation of the characteristics of hydraulic fracture initiation by using maximum tangential stress criterion. *J. Min. Strata Control Eng.* 3 (2), 023520. doi:10.13532/j.jmsce.cn10-1638/td.20201217.001

Zheng, H., Zhang, J., and Qi, Y. (2020). Geology and geomechanics of hydraulic fracturing in the Marcellus shale gas play and their potential applications to the Fuling shale gas development. *Energy Geosci.* 1 (1–2), 36–46. doi:10.1016/j.engeos.2020.05.002

Zhu, W., Niu, L., and Li, S. (2019). Creep-impact test of rock: Status-of-the-art and prospect. *J. Min. Strata Control Eng.* 1 (1), 013003. doi:10.13532/j.jmsce.cn10-1638/td.2019.02.007